International Journal of Engineering and Applied Physics (IJEAP)
Vol. 5, No. 3, September 2025, pp. 1232~1240
ISSN: 2737-8071

On the Dynamics and Heat Transfer of a Conducting Droplet during Electrospraying in the Dripping Mode

Reza Khanpour, Pedram Pournaderi
Department of Mechanical Engineering, Yasouj University, Yasouj, Iran

Article Info

Article history:

Received Jul 9, 2025
Revised Aug 11, 2025
Accepted Aug 21, 2025

Keywords:

Electric Field
Electrospray
Heat Transfer
Dripping Regime
Conducting Liquid

ABSTRACT

In this study, the influence of an applied electric field on the hydrodynamic and heat transfer of a conducting liquid exiting from a nozzle in the dripping regime is investigated. The flow and energy equations along with the electrostatic equations are solved to simulate this problem. The sharp formulation of the level set technique is implemented to capture the interface accurately. Subjected to an electric field, the liquid is exited faster and its elongation before detachment of the droplet is increased. Also, after the first droplet detaches, the liquid returns towards the nozzle. The length of the exited liquid after returning towards the nozzle increases under an electric field. Therefore, under electric stresses, the droplet formation occurs faster due to the rapid exit and more elongation of the liquid. Also, the size of the formed droplet is reduced with electric field intensity. Under an electric field, the heat transfer rate enhances rapidly in a short time interval before droplet detachment. The total heat transferred to the liquid exited from the nozzle is reduced by increasing the electric field intensity.

Corresponding Author:

Pedram Pournaderi,
Department of Mechanical Engineering,
Yasouj University,
Yasouj, Iran.
Email: sp.pournaderi@yu.ac.ir

1. INTRODUCTION

The electrospray is a phenomenon in which the application of an electric field to a liquid exiting from a nozzle results in the liquid breakup and droplet formation. Due to the ability for decreasing the droplet size to the nanoscale, this method is widely used compared to other spraying methods. Therefore, understanding of this phenomenon can lead to the better control over the hydrodynamic behaviors of the liquid during spraying process. This ultimately results in the formation of droplets with desired sizes.

Sung and Lee [1] experimentally studied the formation of small liquid droplets by varying some effective parameters in the electrohydrodynamic spraying process, including liquid flow rate and field strength. They observed that enhancing the voltage enhances the liquid thread length in the jetting mode while reducing the average droplet radius. Also, increasing the flow rate increases the liquid thread length. Sen et al. [2] modeled the electrospraying process for a fluid with negligible conductivity. They solved the equation of electric charge transport to determine the distribution of charges during the process. They utilized the VOF technique to model the interface and examined the effect of flow rate and electric conductivity on the jet diameter. They observed that by increasing the electric conductivity, the jet diameter decreases. Also, by enhancing the flow rate, the jet diameter increases. Collins et al. [3] conducted a numerical study using the finite element approach to investigate the behavior of a liquid jet. They found that the electric forces reduce

the breakup time of the liquid. Lim et al. [4] studied the cone jet formation phenomenon using the front tracking technique. They concluded that the jet diameter decreases with increasing the applied electric potential. Hokmabad et al. [5] examined the electrohydrodynamic of a liquid jet in the presence of a transverse electric field to gain a precise understanding of the formation of secondary droplets which are undesired in the inkjet printing. They concluded that by increasing the voltage intensity the deviation and rupture of the liquid jet increase, but the length of the liquid jet remains unchanged. Kamali and Dehghan Manshadi [6] simulated the formation of microdroplets based on the leaky dielectric theory and found that, depending on the liquid electric properties, the volume of the formed microdroplets may increase or decrease compared to the case that the electric field is not applied. Borthakur et al. [7] focused on the electrohydrodynamic of the drop formation from an orifice. Their simulations showed that by using the suitable electric field, the desired volume of the detached droplet can be achieved. Rosell-LIompart et al. [8] analyzed the electrospraying in the cone jet regime experimentally. They tried to describe the underlying physics of this process by developing the relations connecting different variables called the scaling laws. Guo et al. [9] studied the drop formation in the dipping regime through both experiment and numerical simulation. They found that the charge relaxation time of liquid exited from the nozzle has an important effect on the characteristics of the formed satellite droplets. Wang et al. [10] employed experiment and theory to study electrohydrodynamic atomization and reported an increase in the dripping frequency and a decrease in the droplet radius subjected to an electric field. Panahi et al. [11] used the experiment to investigate the behavior of viscoelastic polymeric solutions in the electrospraying process. It was shown that the extent of the dripping mode in the operating map decreases with solution concentration. Wang et al. [12] conducted an experiment and studied the meniscus oscillations induced by an electric field in the dripping mode. They observed an enhancement in the oscillation frequency after droplet detachment by increasing the electric field intensity. Kim and Hong [13] examined the influence of liquid electric conductivity on the atomization process. They reported that the Sauter mean diameter of the jet increases with the liquid flow rate. Hathi et al. [14] focused on the electrohydrodynamic breakup of a liquid jet. Their simulations revealed the important effect of the electric Bond number on the formation frequency and diameter of the droplets.

In this study, the hydrodynamic and heat transfer of a conductive liquid exiting from a nozzle in the dripping mode is investigated. The above literature review indicates that the numerical works on this subject are limited. The available works mainly have focused on this phenomenon based on the leaky dielectric theory without considering the heat transfer aspects. In this study, both hydrodynamic and heat transfer of a highly conducting liquid exiting from a nozzle is studied based on the perfect conductive model.

2. EQUATIONS

2.1. Flow and energy equations

Given the incompressibility of phases, the conservation equations for mass and momentum are expressed as follows:

$$\nabla \cdot \boldsymbol{u} = 0 \tag{1}$$

$$\frac{\partial \boldsymbol{u}}{\partial t} + \boldsymbol{u}.\nabla \boldsymbol{u} = -\frac{1}{\rho}\nabla p + \frac{1}{\rho}\nabla.(\boldsymbol{\tau}^H + \boldsymbol{\tau}^E) + \boldsymbol{g} \tag{2}$$

The above relation involves the velocity vector $\boldsymbol{u}$, density ρ, pressure p, gravitational vector $\boldsymbol{g}$, time t, the tensor of viscous stress $\boldsymbol{\tau}^H$, and the tensor of Maxwell stress $\boldsymbol{\tau}^E$. The viscous and Maxwell tensors are computed as:

$$\tau^H = \mu(\nabla \boldsymbol{u} + \nabla \boldsymbol{u}^T) \tag{3}$$

$$\tau^E = \varepsilon(\boldsymbol{EE} - \frac{1}{2}\boldsymbol{E} \cdot \boldsymbol{EI}) \tag{4}$$

In equations (3) and (4), $\boldsymbol{\mu}$, $\boldsymbol{\varepsilon}$, and $\boldsymbol{E}$ are dynamic viscosity, electric permittivity, and electric field vector, respectively.

The temperature field is computed from:

$$\frac{\partial T}{\partial t} + \boldsymbol{u}.\nabla T = \frac{1}{\rho C_p}\nabla.(k\nabla T) \tag{5}$$

In equation (5), T, k, and C_p stand for temperature, conductivity and specific heat, respectively.

2.2. Electrostatic equations

The electric field is defined as the amount of electric force per unit positive electric charge at a specific point in the space. Considering the non-rotational nature of the electric field vector ($\nabla \times \boldsymbol{E} = 0$) [15]:

$$\boldsymbol{E} = -\nabla \Psi \tag{6}$$

where Ψ depicts the electric potential. Without a magnetic field:

$$\nabla.(\varepsilon \boldsymbol{E}) = 0 \tag{7}$$

As a result, equation (7) is rewritten as:

$$\nabla.(\varepsilon \nabla \Psi) = 0 \tag{8}$$

Conductive fluids contain electric carriers in the form of free charges or ions. When these fluids are subjected to an electric field, ions or free electrons migrate from the volume of the fluid toward its surface. Therefore, the electric field inside a conducting fluid is zero and the electric field equation is solved only for the surrounding fluid. In conductive materials, since the interface has a constant electric potential, applying an electric field only leads to normal electric stresses.

2.3. Interfacial jump conditions

In two-phase flow problems, the values of physical parameters across both sides of the interface vary, leading to a jump at the interface. The jump in "A" at the interface Γ is shown by equation (9):

$$[A]_\Gamma = A^+ - A^- \tag{9}$$

The positive superscript indicates the region outside the interface and the negative superscript denotes the region inside the interface. Based on the governing equations at the interface, the interfacial jumps are written as follows [15]:

$$\left[\begin{pmatrix} \boldsymbol{n} \\ \boldsymbol{t} \end{pmatrix}\left(p\boldsymbol{I} - (\boldsymbol{\tau}^H + \boldsymbol{\tau}^E)\boldsymbol{n}^T\right)\right]_\Gamma = \begin{pmatrix} \gamma\kappa \\ 0 \end{pmatrix} \tag{10}$$

where κ and γ are curvature and surface tension, respectively. Assuming the flow is viscous and substituting the stress tensors into equation (10), equations (11) and (12) can be derived:

$$\left[\boldsymbol{p} - 2\mu\boldsymbol{n}^{\boldsymbol{T}} \cdot \nabla\boldsymbol{u} \cdot \boldsymbol{n}\right]_\Gamma - \boldsymbol{n} \cdot \left[\varepsilon\left(\boldsymbol{EE} - \frac{1}{2}\boldsymbol{E} \cdot \boldsymbol{EI}\right)\right]_\Gamma \cdot \boldsymbol{n}^{\boldsymbol{T}} = \gamma\kappa \tag{11}$$

$$\boldsymbol{t} \cdot \left[\mu\left(\nabla\boldsymbol{u} + \nabla\boldsymbol{u}^T\right)\right]_\Gamma \cdot \boldsymbol{n}^T + \boldsymbol{t} \cdot \left[\varepsilon\left(\boldsymbol{EE} - \frac{1}{2}\boldsymbol{E} \cdot \boldsymbol{EI}\right)\right]_\Gamma \cdot \boldsymbol{n}^T = 0 \tag{12}$$

Equation (11) expresses the pressure jump condition, while equation (12) represents the jump condition related to viscous stresses at the interface.

From energy balance at the interface, the following jump condition is obtained:

$$[k\nabla T \cdot \mathbf{n}]_\Gamma = 0 \tag{13}$$

The jump conditions for electric potential and displacement (εE) for a conducting medium are as follows:

$$[\Psi]_\Gamma = \Psi_0 \tag{14}$$

$$[\varepsilon\nabla\Psi \cdot \mathbf{n}]_\Gamma = q_s \tag{15}$$

Ψ_0 is the potential of the droplet surface and, q_s is the density of free charges at the interface. Equation (14) states that the interface is an isopotential surface, and equation (15) shows the effect of the surface charge distribution at the interface.

3. NUMERICAL METHODS

The basic equations are discretized by the finite difference technique. Convection terms in the equations are discretized using the WENO method [16] with fifth order accuracy, and diffusion terms are discretized using second order central differencing. Temporal discretization is performed using the Runge-Kutta method [16] with third order accuracy.

The flow equations are solved by the projection technique [16]. The level set method is employed for tracking the interface, and interfacial discontinuities are enforced by the ghost fluid method.

3.1. Level set method

In this method, the position of the interface is represented by a scalar function φ called the level set function. This function for both phases is defined as the minimum distance to the interface with opposite signs in two phases. The level set equation is written as [17]:

$$\frac{\partial \varphi}{\partial t} + \boldsymbol{u}_{\Gamma} \cdot \nabla \varphi = 0 \tag{16}$$

the $\boldsymbol{u}_{\Gamma}$ represents the interface velocity. The function φ is kept as the distance function by solving the following reinitialization equation [18]:

$$\frac{\partial \varphi}{\partial \tau} = S(\varphi_0)\left(1 - |\nabla \varphi|\right) \tag{17}$$

In the above equation, φ_0 is the value of φ before correction and τ is a virtual time. $S(\varphi_0)$ is defined as:

$$S(\varphi_0) = \frac{\varphi_0}{\sqrt{\varphi_0^2 + \left(\max(\Delta x, \Delta y)\right)^2}} \tag{18}$$

3.2. Ghost fluid method

In the studied problem, some quantities are discontinuous across the interface and, therefore, the governing equations including these quantities cannot be discretized in the normal fashion. In the ghost fluid method, each phase is extended into another phase by considering some ghost nodes. These ghost nodes help us to discretize the derivative of discontinuous quantities in the usual manner. The values of discontinuous quantities in ghost nodes are determined using the jump conditions. More details can be found in [16].

4. RESULTS

4.1. Problem definition

In this work, the flow and heat transfer of a conducting liquid exiting from a nozzle in the dripping regime is investigated. Figure 1 indicates a general schematic of the problem. The problem is simulated based on an axisymmetric model. The boundary conditions include symmetry boundary condition on the left boundary, full slip condition on the right and top, outflow condition at the bottom boundary, and no-slip condition on the nozzle wall. The fully developed velocity profile at the inlet boundary of the nozzle is applied, represented by Eq. (19):

$$V = 2V_0\left(1 - \left(\frac{x}{R}\right)^2\right) \qquad 0 \le x \le R \tag{19}$$

In Equation (19), R, V_0, and x are the nozzle radius, the fluid average velocity, and the distance to the

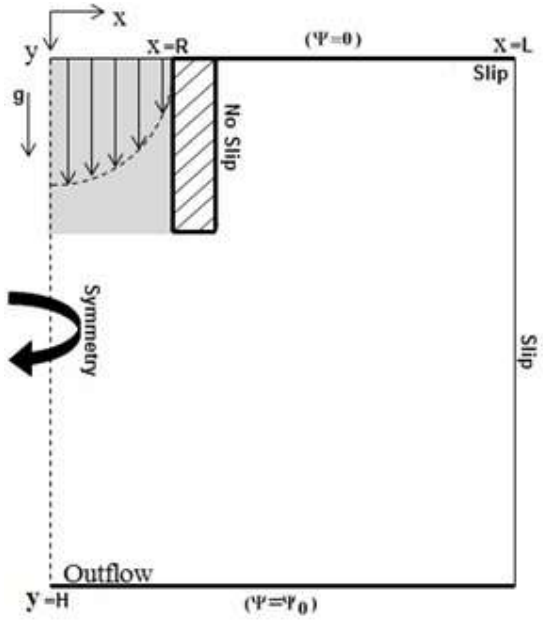

Figure 1. Domain and boundary conditions

Table 1. Physical properties

Property	Inside the Nozzle	Outside the Nozzle
Density (kg.m^{-3})	998	921
Viscosity (Pa.s)	0.001	0.0663
Electric permittivity (Fm^{-1})	708.32e-12	35.4e-12
Specific heat (J.kg^{-1}.K^{-1})	4180	2130
Conductivity (W.m^{-1}.K^{-1})	0.6	0.16
Liquid Temperature (K)	298.15	333.15

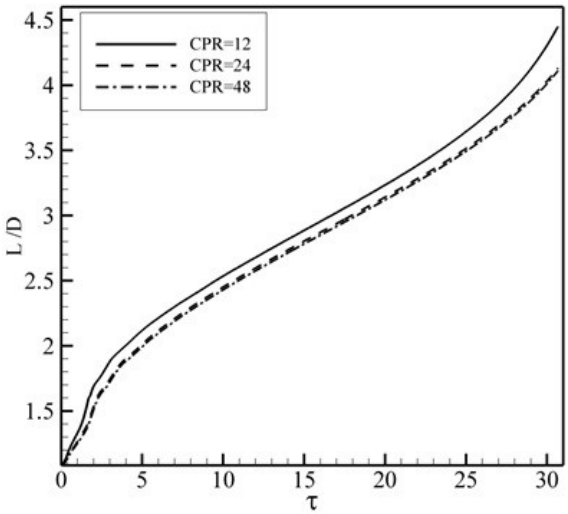

Figure 2. Simulation results for different grids ($Ca_E = 0.3$)

symmetry axis, respectively. A specific electric voltage is applied between the nozzle wall and the bottom boundary. In these simulations, the water is used as the conducting fluid inside the nozzle, while the crude oil is used as the surrounding dielectric fluid. The properties of these liquids have been presented in Table 1. The surface tension is 0.027 Nm^{-1}. In the simulations, the dimensions of the computational domain, L and H, are considered 8R and 12R. The nozzle radius, R, and the fluid average velocity, V_0 are 0.0047m and 0.006 ms^{-1}, respectively.

4.2. Verification of the results

Previously, we have simulated the liquid exit from a nozzle in the dripping mode successfully and studied the effect of important non-dimensional parameters on this phenomenon [19]. Also, in another work, we studied the influence of a uniform field on the hydrodynamic and heat transfer of a stationery conducting droplet [20]. These previous studies confirm the validity of the results extracted from our code for simulating a conducting liquid exiting from a nozzle in the dripping regime under an electric field.

To examine the effect of the grid size, the liquid exit from the nozzle is considered with an electric capillary number $\left(Ca_E = \varepsilon_j E^2 D / \gamma\right)$ of 0.3. D stands for the nozzle diameter, and the subscript j refers to the liquid phase exited from the nozzle. Figure 2 indicates the non-dimensional length of the exited liquid versus non-dimensional time defined as:

$$\tau = \frac{t}{\sqrt{\frac{\rho_j R^3}{\gamma}}} \tag{20}$$

Due to the slight difference between the results obtained for meshes with CPR $(\text{CPR}=\frac{R}{\Delta x})$ of 24 and 48, the mesh with the resolution of CPR=24 is selected for the simulations.

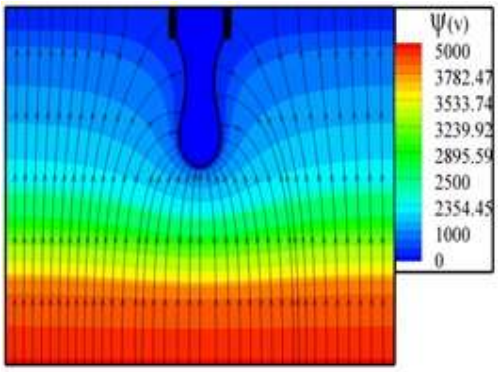

Figure 3. Electric field lines and contours of electric potential ($Ca_E = 2, \tau = 22.27$)

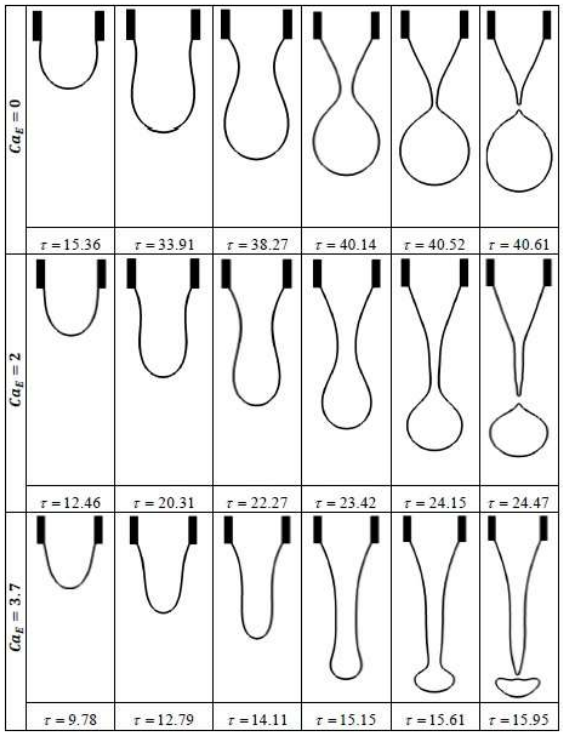

Figure 4. Liquid exit from the nozzle under different electric fields

4.3. Hydrodynamic results

In this section, the influence of the electric field on the hydrodynamic of the conducting liquid exited from the nozzle in the dripping mode is investigated. Figure 3 indicates the profile of the liquid exited from the nozzle at $\tau = 22.27$ under an electric field with the electric capillary number of 2. The field lines and the contours of the electric potential are also observed in this figure. Due to the conductivity of the liquid exited from the nozzle, the interface is an equipotential surface. Therefore, the electric field lines are normal to the interface. The perpendicularity of equipotential surfaces to the far boundaries indicates that the far-field boundary condition is satisfied on these boundaries. The concentration of the field lines at the tip of the exited liquid indicates the higher intensity of the electric forces in this region. Subjected to the electric field, electric charges transfer to the interface rapidly. The higher accumulation of electric charges in the points close to the tip of the exited liquid leads to the higher electric forces at these regions.

Figure 4 indicates the time evolution of the liquid profile when exiting from the nozzle under different electric fields. The conducting liquid exits from the nozzle and is elongated under the influence of the inertia, gravitational, and electric forces. When these forces overcome the surface tension, a small droplet is separated. With an enhancement in the field intensity, the liquid elongation increases, and the size of the

detached droplet decreases. The role of the electric field is to transfer electric charges presented in the conducting liquid volume to the interface. As these electric charges accumulate on the interface, electric forces are generated. An enhancement in electric forces compared to the interfacial forces results in the liquid elongation. This elongation causes a decrease in the diameter of the detached droplet. It should be noted that the droplet detachment under the influence of electric forces occurs faster.

Figure 5 shows the length of the exited liquid versus time. It is evident from this figure that by enhancing the electric capillary number, the length of the exited liquid increases, and the time required for droplet detachment decreases. As it is observed in this figure, after droplet detachment, under the influence of the surface tension, the exited liquid returns towards the nozzle and the length of the exited liquid reduces. It is also observed that with an enhancement in the field intensity, due to the effects of electric stresses, the length of the exited liquid after returning towards the nozzle increases. This phenomenon accelerates the drop formation process.

4.4. Heat transfer results

In this section, the electric field influence on the heat transfer from the ambient fluid to the fluid exiting the nozzle is investigated. The non-dimensional heat transfer rate is computed as:

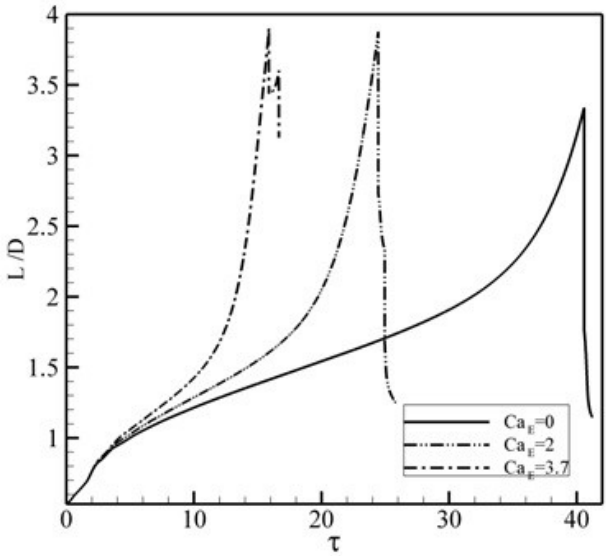

Figure 5. The length of the exited liquid as a function of time for different electric capillary numbers

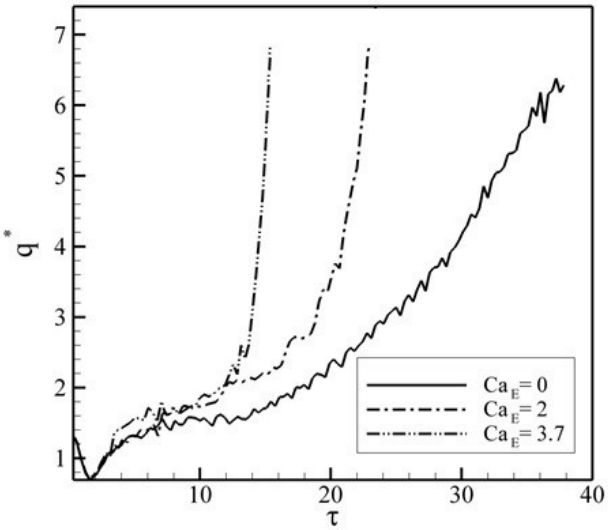

Figure 6. Time variations of the heat transfer rate for various electric capillary numbers

$$q^* = \frac{q_1}{k_j D(T_c - T_j)} \tag{21}$$

T_j and T_c, the initial temperature of liquids inside and outside the nozzle, are 298.15K and 333.15K, respectively. The heat transfer rate, q_1, is calculated as:

$$q_1 = -\int_{A_\Gamma} k \frac{\partial T}{\partial n} dA \tag{22}$$

where A_Γ shows the interface between the phases.

Figure 6 depicts variations of the heat transfer rate (in non-dimensional form) to the fluid exiting the nozzle versus time for several electric capillary numbers until the moment at which the first droplet detaches. Based on the obtained results, at the initial moments the heat transfer rate is almost the same for various electric capillary numbers. However, by advancing in time, the difference between the results becomes higher. As it was observed in Fig. 4, for stronger electric fields, the liquid is exited from the nozzle faster and as a result, the liquid elongation and droplet detachment occurs in a shorter time. Therefore, due to the rapid increase of the interface between the two fluids, the heat transfer rate increases rapidly. Figure 7 indicates the total heat transferred to the liquid exited from the nozzle until $\tau = 40$ (the dimensionless time at which the first droplet detaches when the field is absent) versus the electric capillary number. According to this figure, as the electric filed intensity increases the total heat transfer decreases. Based on Fig. 6, despite the case that the electric field is absent, under an applied electric field, a rapid enhancement in the heat transfer rate occurs in a short time interval. When the electric capillary number increases this effect is intensified. This results in a decrease in the total heat transferred to the exited liquid when the electric field intensity is increased.

5. CONCLUSION

In this work, the flow and heat transfer of a conducting liquid exiting a nozzle in the dripping mode is investigated. The sharp version of the level set technique is adopted to capture the interface accurately. In this case, the ghost fluid method in combination with the level set method is utilized to impose jump condition across the interface.

Subject to the electric forces, the elongation of the liquid exited from the nozzle before droplet detachment increases. Moreover, liquid exit and elongation occur in a shorter time. Also, after droplet formation the liquid is returned towards the nozzle less compared to the case that the electric field is not present. Therefore, due to the rapid exit of the liquid and its more elongation, the drop formation occurs faster. Also, the size of the formed droplet decreases with the electric field intensity. When the electric field is applied, the heat transfer rate increases in a short interval just before the droplet detachment, nevertheless, the total heat transferred to the liquid exited from the nozzle decreases with electric field intensity.

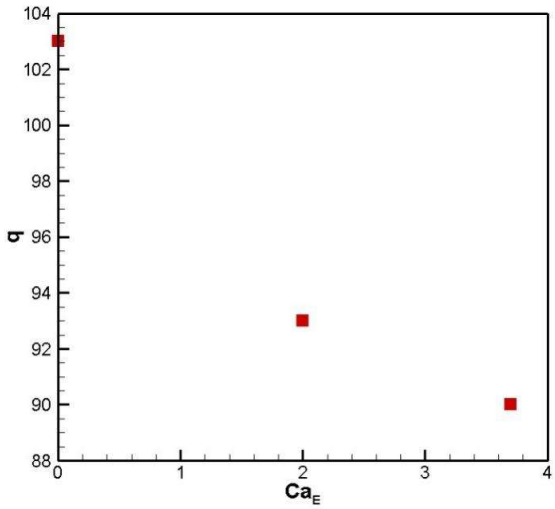

Figure 7. Total heat transfer until $\tau = 40$ versus electric capillary number

REFERENCES

[1] K. Sung and C. S. Lee, "Factors Influencing Liquid Breakup in Electrohydrodynamic Atomization," *Journal of Applied Physics*, vol. 96, pp. 3956–3961, 2004. https://doi.org/10.1063/1.1790062

[2] A. K. Sen, *et al*., "Modeling and Characterization of a Carbon Fiber Emitter for Electrospray Ionization," *Journal of Micromechanics and Microengineering*, vol. 16, pp. 620, 2006.

[3] R. T. Collins, *et al*., "Breakup of Electrified Jets," *Journal of Fluid Mech*anics, vol. 588, pp. 75-129, 2007. https://doi.org/10.1017/S0022112007007409

[4] L. K. Lim, *et al*., "Numerical Simulation of Cone-jet Formation in Electrohydrodynamic Atomization," *AIChE Journal*, vol. 57, pp. 57-78, 2011. https://doi.org/10.1002/aic.12254

[5] B. V. Hokmabad, *et al*., "Electric Field-assisted Manipulation of Liquid Jet and Emanated Droplets," *International Journal of Multiphase Flow*, vol. 65, pp. 127-137, 2014. https://doi.org/10.1016/j.ijmultiphaseflow.2014.03.009

[6] R. Kamali and M. K. Dehghan Manshadi, "Numerical Simulation of the Leaky Dielectric Microdroplet Generation in Electric Fields," *International Journal of Modern Physics. C*, vol. 27, pp. 1650012, 2016. https://doi.org/10.1142/S0129183116500121

[7] M. P. Borthakur, *et al*., "Dynamics of Drop Formation from Submerged Orifices under the Influence of Electric Field," *Physics of Fluids*, vol. 30, pp. 30, 2018. https://doi.org/10.1063/1.5063913

[8] J. Rosell-Llompart, *et al*., "Electrosprays in the Cone-jet Mode: From Taylor Cone Formation to Spray Development," *Journal of Aerosol Science*., vol. 125, pp. 2-31, 2018. https://doi.org/10.1016/j.jaerosci.2018.04.008

[9] L. Guo, *et al*., "Charged Satellite Drop Avoidance in Electrohydrodynamic Dripping," *Micromachines,* vol. 10, pp. 172, 2019. https://doi.org/10.3390/mi10030172

[10] Z. Wang, et al., "Formation of Mono-dispersed Droplets with Electric Periodic Dripping Regime in Electrohydrodynamic (EHD) Atomization," *Chinese Journal of Chemical Engineering*, vol. 28, pp. 1241-1249, 2020. https://doi.org/10.1016/j.cjche.2020.03.008

[11] A. Panahi, *et al*., "Experimental Investigation of Electrohydrodynamic Modes in Electrospraying of Viscoelastic Polymeric Solutions," *Physics of Fluids*, vol. 32, 2020. https://doi.org/10.1063/1.5132556

[12] Z. Wang, *et al*., "Dynamics of Droplet Formation with Oscillation of Meniscus in Electric Periodic Dripping Regime," *Experimental Thermal and Fluid Science*, vol. 120, pp. 110250, 2021. https://doi.org/10.1016/j.expthermflusci.2020.110250

[13] J. Y. Kim and J. G. Hong, "Effect of Electrical Conductivity on Atomization Characteristics of Electrospray," *Journal of Applied Fluid Mech*anics, vol. 15, pp. 1427-1436, 2022. https://doi.org/10.47176/jafm.15.05.1094

[14] D. S. Hathi, *et al*., "A Numerical Study on Breakup of a Liquid Jet in an Axial Electric Field," *Journal of Aerosol Science*, vol. 170, pp. 106142, 2023. https://doi.org/10.1016/j.jaerosci.2023.106142

[15] H. Nazari and P. Pournaderi, "The Electric Field Effect on the droplet Collision with a Heated Surface in the Leidenfrost Regime," *Acta Mechanica*, vol. 230, pp. 787-804, 2019. https://doi.org/10.1007/s00707-018-2323-z

[16] M. Kang, *et al*., "A Boundary Condition Capturing Method for Multiphase Incompressible Flow," *Journal of Scientific Computing*, vol. 15, pp. 3230360, 2000. https://doi.org/10.1023/A:1011178417620

[17] M. Shen and B. Q. Li, "A 3D Conservative Level set Model to Simulate Drop Impact with Phase Change onto Solid Surfaces," *International Journal of Multiphase Flow,* vol. 169, pp. 104615, 2023. https://doi.org/10.1016/j.ijmultiphaseflow.2023.104615

[18] M. Emdadi and P. Pournaderi, "Study of Droplet Impact on a Wall Using a Sharp Interface Method and Different Contact Line Models," *Journal of Applied Fluid Mechanics*, vol. 12, pp. 1001-1012, 2019. https://doi.org/10.29252/JAFM.12.04.29029

[19] R. Khanpour and P. Pournaderi, "Simulation of the Liquid Spraying Process in the Dripping Mode by Using the Level-Set Method," *Amirkabir Journal of Mechanical Engineering*, vol. 52, pp. 847-862, 2019. https://doi.org/10.22060/mej.2019.14689.5914

[20] H. Nazari and P. Pournaderi, "Simulation of Hydrodynamic Behavior of a Conductive Drop under an Electric Field," *Amirkabir Journal of Mechanical Engineering*, vol. 51, pp. 297-312, 2019. https://doi.org/10.22060/mej.2017.12700.5400